

# Enhanced Athermal Phonon Responsivity in a Kinetic Inductance Detector with Integrated Phonon Collectors

L. Pesce , <sup>a)</sup> A.L. De Santis , <sup>1, 2, b)</sup> M. Calvo , <sup>3</sup> M. Cappelli , <sup>1, 2</sup> U. Chowdhury, <sup>3</sup> A. Cruciani , <sup>2</sup> G. Del Castello , <sup>2</sup> D. Delicato , <sup>3, 1, 2</sup> M. Folcarelli , <sup>1, 2</sup> M. del Gallo Roccagiovine , <sup>1, 2</sup> A. Monfardini , <sup>3</sup> D. Quaranta , and M. Vignati 

<sup>1)</sup> Dipartimento di Fisica - Sapienza Università di Roma - Piazzale Aldo Moro 2, 00185, Roma, Italy

<sup>2)</sup> INFN - Sezione di Roma - Piazzale Aldo Moro 2, 00185, Roma, Italy

<sup>3)</sup> Univ. Grenoble Alpes, CNRS, Grenoble INP, Institut Néel, 38000 Grenoble, France

(Dated: 14 January 2026)

Cryogenic phonon detectors are adopted in light dark matter searches and coherent elastic neutrino-nucleus scattering experiments as they can achieve low energy thresholds. The phonon mediated sensing of silicon particle absorbers has already been proved with Kinetic Inductance Detectors (KIDs), acting both as sensors and athermal phonon absorbers at the same time. In this work we present the design and the performance of an improved detector, where the KID acts only as sensor and is coupled to dedicated phonon collectors. The separation between the detector and the collectors increases the variation of the quasi-particle density within the device, thereby enhancing its responsivity. The meander of the KID is composed of a 77 nm trilayer wire of Aluminum-Titanium-Aluminum, while the phonon collectors are made of a 100 nm Aluminum layer and act as quasi-particles funnels. Inside the collectors, the absorbed athermal phonons generate quasi-particles which, after diffusion, are trapped in the lower-gap superconducting trilayer. The performance of this setup is compared to that of a standard phonon-mediated KID, showing an increase in responsivity by around a factor of five.

The following article has been submitted to Applied Physics Letters. Copyright 2026 Leonardo Pesce, Alessio Ludovico De Santis, Martino Calvo, Matteo Cappelli, Usasi Chowdhury, Angelo Cruciani, Giorgio Del Castello, Daniele Delicato, Matteo Folcarelli, Matteo del Gallo Roccagiovine, Alessandro Monfardini, Davide Quaranta, and Marco Vignati. This article is distributed under a Creative Commons Attribution (CC BY) License.

Experiments searching for direct light dark matter interaction<sup>1–3</sup> or coherent elastic neutrino-nucleus scattering<sup>4–8</sup> have to address two main technological challenges: the need for high sensitivity to nuclear recoils and the scaling of the instrumented target mass.

The small nuclear recoil energies require detectors with energy thresholds as low as possible. For this reason, cryogenic detectors such as Transition Edge Sensors (TESs)<sup>1,4,9</sup> or Neutron Transmutation Doped (NTD) Germanium thermistors<sup>2,6</sup> are adopted as phonon sensors coupled to target crystals, in order to detect sub-keV nuclear recoil processes. Energy thresholds of the order of 1 – 10 eV have already been achieved<sup>4,9,10</sup>.

At the same time, the development of mass-scalable instruments is essential for achieving detectors with improved sensitivity to increasingly smaller dark-matter interaction cross sections, assuming a Weakly Interacting Massive Particle (WIMP) model. Experiments with target mass of tens of grams have been built<sup>1,4,11</sup>, but scaling-up to the kilogram still remains an experimental challenge.

The BULLKID project developed a particle detector designed for tackling the mass scaling problem<sup>12</sup>. It

consists of a monolithic array of 60 silicon dices, each one with mass of 0.34 g and volume  $5.4 \times 5.4 \times 5 \text{ mm}^3$ , carved from a wafer with a diameter of 7.6 cm and 5 mm thickness. The dices are sensed with 60 KIDs acting as phonon-mediated particle detectors. These are well suited for use in large arrays due to their intrinsic multiplexing capability<sup>13</sup> and therefore can be adopted to design mass-scalable instruments. BULLKID achieved an energy resolution of 27 eV — which led to set an analysis threshold of around 160 eV<sup>14</sup> — that is still far from the current state of art of the other cryogenic detectors. For this reason, it is important to design and develop new sensors aimed at lowering the energy threshold, to the greatest extent possible. In this letter, we investigate a KID design aimed at achieving this goal.

KIDs, which were originally developed for the detection of optical<sup>15</sup> and millimeter-wavelength<sup>16</sup> light, have found application also as phonon-mediated particle detectors<sup>12,17–19</sup>. A KID is a superconducting LC resonator<sup>20</sup> in which the total inductance  $L$  is the sum of two contributions: the magnetic inductance  $L_g$ , which is related to the geometry of the superconductor, and the kinetic inductance  $L_k$ , which is associated to the Cooper Pairs (CPs) motion inside the metal and depends on their number density. When energy  $E$  is released in the substrate onto which the phonon-mediated KID is deposited, athermal phonons are generated and absorbed by the KID itself. If the phonon energy  $E_{\text{ph}}$  satisfies  $E_{\text{ph}} > 2\Delta_0$ , where  $\Delta_0 \simeq 1.76k_B T_c$  is the superconducting gap of the metal,  $k_B$  the Boltzmann constant and  $T_c$  the critical temperature<sup>20</sup>, CPs in the superconductor are broken and Quasi-Particles (QPs) are generated. This process reduces the CP number density, which in turn increases the kinetic inductance  $L_k$ , leading to a

<sup>a)</sup> Electronic mail: [leonardo.pesce@uniroma1.it](mailto:leonardo.pesce@uniroma1.it)

<sup>b)</sup> now at Gran Sasso Science Institute (GSSI), 67100, L'Aquila, Italy

resonant frequency shift,  $\Delta f_r$ , and to a reduction of the resonance depth<sup>20–24</sup>.

The change of the CP density is detected by monitoring the phase and magnitude modulation of the complex single pole transmission function  $S_{21}(\Delta f_r)$  of the resonator<sup>25</sup>:

$$S_{21}(\Delta f_r) = 1 - \frac{Q}{Q_c} \frac{1}{1 + 2jy} \quad (1)$$

where  $Q = (Q_c^{-1} + Q_i^{-1})^{-1}$  is the total quality factor of the resonator, which combines the coupling quality factor  $Q_c$  and the internal quality factor  $Q_i$ , that accounts for internal losses due to imperfections and thermal QPs population within the sensor. Finally, the parameter  $y = Q \cdot \Delta f_r / f_r$  is the detuning of the readout frequency relative to the resonance width<sup>20,21,24</sup>. Usually, the phase readout  $\varphi$  provides a better signal-to-noise ratio<sup>20</sup>; therefore, this will be adopted in this work.

The signal responsivity  $r$  of a KID in terms of  $\varphi$  is<sup>20,21,25–27</sup>:

$$r = \frac{d\varphi}{dE} = \frac{\eta}{V_{\text{KID}}} \frac{\alpha S_2(f_r, T) Q}{N_0 \Delta_0^2} \frac{1}{1 + 4y^2} \quad (2)$$

where  $\eta$  is the energy to pair-breaking conversion efficiency,  $V_{\text{KID}}$  is the active volume of the sensor,  $\alpha = L_k/(L_k + L_g)$  is the fraction of kinetic inductance,  $S_2(f_r, T)$  is a dimension-less function of order 1 coming from the Mattis-Bardeen theory and  $N_0$  is the the single-spin density of states. We emphasize that in Eq. 2 the term  $\Delta_0$  appears quadratically as the product of two identical gap factors,  $\Delta_0 \cdot \Delta_0$ : the first  $\Delta_0$  arises from the number of CPs broken by a given energy deposition  $E$ , which scales as  $E/\Delta_0$ , while the second  $\Delta_0$  originates from the single-spin volume density,  $N_0 \Delta_0$ , within the sensor<sup>20,21,26,27</sup>.

If the phonons absorption is not saturated and losses due to supports or interfaces do not dominate, the efficiency  $\eta$  scales almost linearly with the phonon collection volume  $V_{\text{ph}}$ <sup>28–30</sup>:

$$\eta \propto V_{\text{ph}} \quad (3)$$

In a standard phonon-mediated KID, the volume  $V_{\text{ph}}$  coincides with that of the active sensor  $V_{\text{KID}}$ , since the phonons generated in the substrate are directly absorbed by the inductor. Consequently, from Eq. 2 it follows that the responsivity  $r$  of the KID weakly depends on  $V_{\text{KID}}$ , thus tuning the active sensor volume alone is not expected to lead to a significant improvement in the detector responsivity. In contrast, the separation of these two volumes would allow to design a device with a large  $V_{\text{ph}}$  and a small  $V_{\text{KID}}$  at the same time, which would enhance the detector responsivity.

We developed and tested a phonon-mediated KID with separate phonon collectors<sup>30–32</sup> that act also as QPs funnels (see Fig. 1). Henceforth, we will refer to this device as the FunKID and to the phonon collectors as the funnels. The resonator is composed of a 77 nm trilayer meander of Aluminum-Titanium-Aluminum (AlTiAl), with

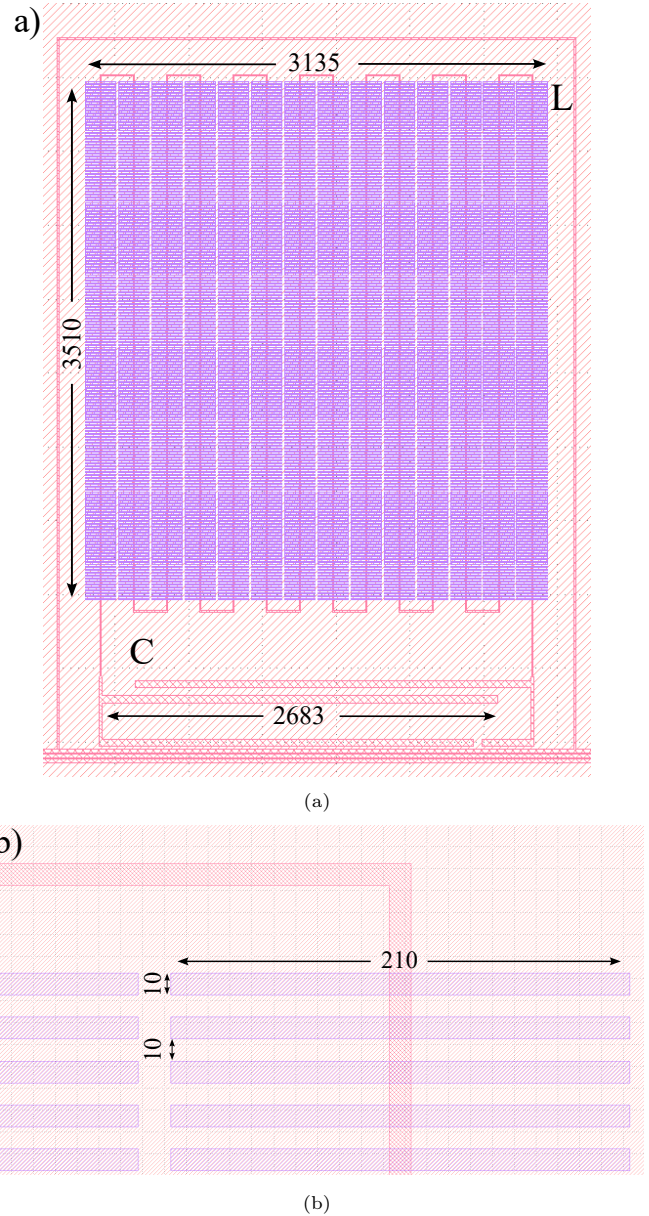


FIG. 1: (a) Layout of the FunKID. The funnels in purple intersect the inductive meander indicated with L. The capacity C is adjusted by means of the first two capacitors to tune the resonant frequency. (b) Detail of the funnels. The measures are in  $\mu\text{m}$ .

14 nm – 33 nm – 30 nm thicknesses, respectively<sup>33</sup>. The inductive part of the KID is composed of seven fingers of around  $3600 \mu\text{m} \times 10 \mu\text{m}$ , evenly spaced by  $215 \mu\text{m}$  (Fig. 1a). The funnels are Aluminum structures with  $210 \mu\text{m} \times 10 \mu\text{m} \times 100 \text{ nm}$  volume intersecting the inductor, evenly spaced by  $10 \mu\text{m}$  (Fig. 1b). The total phonon collection volume, which coincides with the total volume of the funnels, is  $V_{\text{ph}} \simeq 5.2 \text{ mm}^2 \times 100 \text{ nm}$ , while the active volume of the sensor is  $V_{\text{KID}} \simeq 0.55 \text{ mm}^2 \times 77 \text{ nm}$ , giving a volume ratio of  $V_{\text{ph}}/V_{\text{KID}} \simeq 12$ .

Due to proximity effects<sup>33–36</sup> among the two Aluminum layers ( $T_c \simeq 1.2 \text{ K}$ <sup>35</sup>) and the central Titanium

layer ( $T_c \simeq 0.4$  K<sup>35</sup>), the AlTiAl sensor has an intermediate critical temperature  $T_c$ , which is lower than that of the funnels, made of Aluminum. Generally, the AlTiAl critical temperature depends on the boundary resistivities conditions between the layers, and on their thicknesses<sup>37</sup>. For the same design thicknesses, the CALDER project obtained a value of  $T_c \simeq 0.81$  K<sup>33,38</sup>, which is expected also for this resonator, provided that the boundary resistance conditions are sufficiently similar.

In this design, schematically reported Fig. 2a, the athermal phonons produced in the substrate are mostly absorbed by the funnels, where they can break CP generating QPs, which, through diffusion, reach the sensor. Due to the energy gap difference between funnels with gap  $\Delta_{\text{Al}}$  and sensor with gap  $\Delta_{\text{AlTiAl}}$ , QPs with energy  $\Delta_{\text{Al}}$  relax down to  $\Delta_{\text{AlTiAl}}$  and are trapped within the sensor, preventing their recombination in the funnels<sup>31,39</sup>.

The length of the funnels was chosen to be smaller than the characteristic QP diffusion length in aluminum,  $\lambda_r = \sqrt{D\tau_r}$ <sup>40</sup>, where  $D$  is the QP diffusion coefficient and  $\tau_r$  the QP recombination time. We adopted a diffusion coefficient of  $D = 22.5$  cm<sup>2</sup>/s<sup>41</sup>, a conservative choice compared to higher values reported in the literature<sup>42</sup>. The recombination time  $\tau_r$  depends on both film thickness and temperature, and we adopted  $\tau_r \simeq 1$  ms<sup>43,44</sup>, yielding a diffusion length of  $\lambda_r \simeq 1.5$  mm, much higher than half the length of the funnels of 100  $\mu$ m. We can also define a characteristic time scale that quantifies the maximum diffusion time of QPs inside the funnels,  $\tau_{\text{diff}} \sim l^2/D = 4$   $\mu$ s, where  $l = 100$   $\mu$ m is half of the funnel length and corresponds to the maximum distance a QP travels before reaching the sensor. This sets the minimum timescale over which the sensor needs to integrate the signal.

We highlight that the funnels have been designed to be as electrically inert as possible, as shown in the simulation performed with the SONNET software<sup>45</sup> reported in Fig 2b. In particular, the current of the sensor flows through the inductive meander, while only a small fraction leaks in the funnels. However, we notice that possible limitations of the simulations may arise from the modeling of the overlap region between the funnels and the resonator.

We also notice that in the FunKID the separation between phonon absorbers and sensor modifies the term  $\Delta_0^2$  of Eq. 2. In this design, the CPs breaking occurs in the funnels, with gap  $\Delta_{\text{Al}}$ , while the QPs population refers to that of the sensor, with gap  $\Delta_{\text{AlTiAl}}$ . Therefore, the term  $\Delta_0^2$  is replaced by  $\Delta_{\text{Al}}\Delta_{\text{AlTiAl}}$ .

According to the simulation performed with SONNET, the FunKID is designed to have a small coupling quality factor  $Q_c = 20$  k and resonant frequency  $f_r = 1009.6$  MHz, corresponding to an expected ring time  $\tau_{\text{ring}} = Q/\pi f_r = 5$   $\mu$ s<sup>12</sup>. This is the integration time of the sensor and thus should be higher than the diffusion time  $\tau_{\text{diff}}$ , in order to maximize the signal in the sensor. In our case, these time constants are comparable, nega-

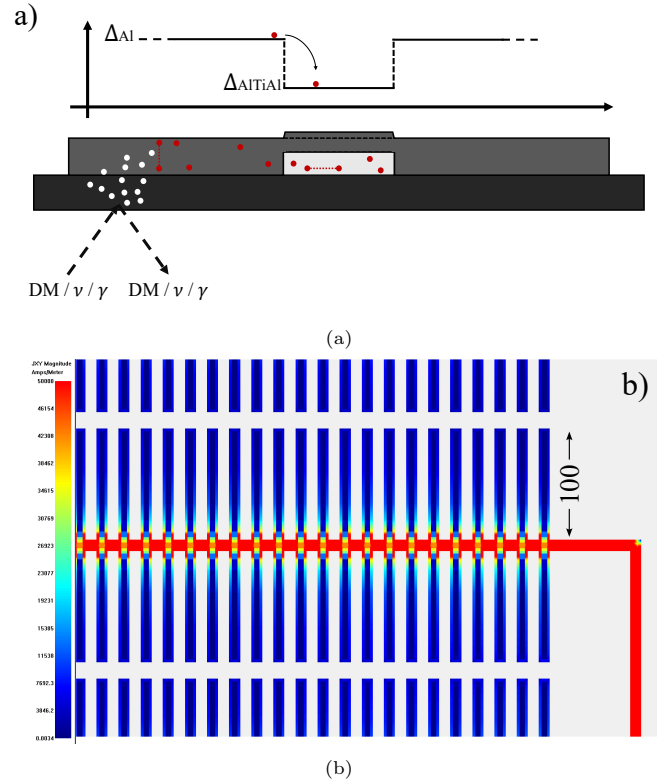


FIG. 2: (a) Detection scheme of the FunKID. Athermal phonons (white dots) are generated by an energy deposition in the substrate. A fraction of these phonons is absorbed by the funnels, which have a higher superconducting gap  $\Delta_{\text{Al}}$ . There, CPs (red paired dots) are broken, producing QPs (single red dots). Finally, the QPs diffuse into the funnel and are absorbed by the KID, which features a lower gap  $\Delta_{\text{AlTiAl}}$ , where they recombine. (b) Current density simulated with SONNET. Most of the current flows into the KID, while a small leakage is observed. The length reported is measured in  $\mu$ m.

tively impacting on the amplitude of the signal. However, the choice of operating with small quality factor lies on possible limitations of the internal quality factor  $Q_i$ <sup>20,31</sup>, which not only would limit the total quality factor  $Q$ , but also would broaden the width and decrease the depth of the resonance, as follows from Eq. 1.

We estimated the gain in responsivity of the FunKID relative to an identical standard KID without funnels,  $r_{\text{FunKID}}/r_{\text{KID}}$ , using the Eq. 2:

$$\frac{r_{\text{FunKID}}}{r_{\text{KID}}} \sim \frac{V_{\text{ph}}}{V_{\text{KID}}} \frac{\alpha_{\text{FunKID}}}{\alpha_{\text{KID}}} \frac{Q_{\text{FunKID}}}{Q_{\text{KID}}} \frac{\Delta_{\text{Al}}}{\Delta_{\text{AlTiAl}}} \quad (4)$$

where we assumed that  $N_0$  and  $S_2(f_r, T)$  were approximately equal among the two devices and that their response was linear, thus  $1 + 4y^2 \simeq 1$ . Moreover, we considered only the geometric dependence of  $\eta$  for both the KIDs according to Eq. 3 and that the phonon collection volume of the standard KID coincides with its active volume  $V_{\text{KID}}$ . In order to evaluate the best gain in responsivity, we assumed same quality factors  $Q$  and kinetic inductance fractions  $\alpha$  for both the devices and the

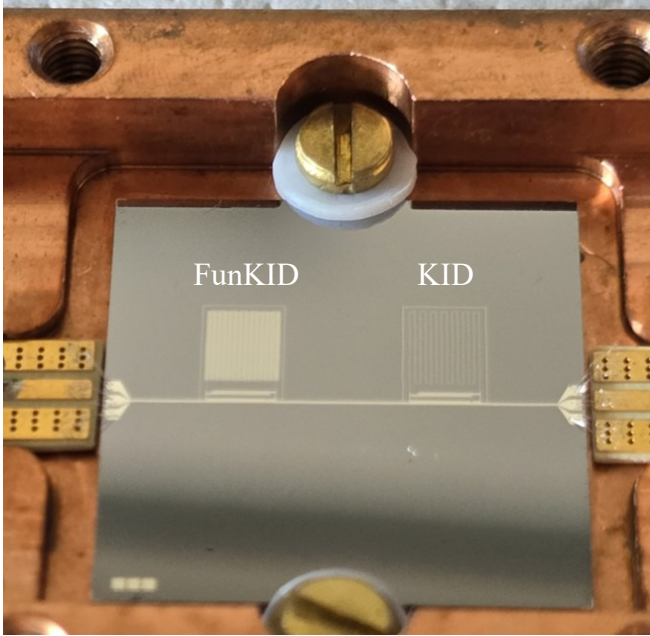


FIG. 3: The two pixels on the silicon tile suspended by Teflon supports. On the left is the FunKID, while on the right the standard phonon-mediated KID.

critical temperatures of Aluminum and AlTiAl of 1.2 K and 0.81 K, respectively. Under these conditions, the expected gain amounts to about 8.

The test device was fabricated at the PTA facility clean room in Grenoble<sup>46</sup> using a 500  $\mu\text{m}$  thick silicon tile. On the same substrate, a standard phonon-mediated KID was produced along with the FunKID (Fig. 3). The KID sensors were etched from a trilayer of Aluminum (30 nm), Titanium (14 nm) and Aluminum (13 nm) following a standard lithographic technique. After the fabrication of the KIDs, photo-resist was used to coat the surface of the wafer, and gaps in the shape of the funnels were patterned on it. The funnels were then realized by selectively depositing 100 nm of Aluminum in the patterned gaps, following a lift-off process. The two resonators are identical except for the first two capacitors length: in the FunKID these were designed 105  $\mu\text{m}$  longer to lower its resonant frequency by approximately 20 MHz with respect to the KID. Finally, we highlight that the feed-line is fabricated from the same AlTiAl trilayer used for the meanders of the two KIDs.

The tile was mounted into a copper holder by means of Teflon supports and wire bonded to 50  $\Omega$  launchers. The device was operated in a dilution  $^3\text{He}/^4\text{He}$  cryostat, at a base temperature  $T_0 \simeq 35\text{ mK}$ , much lower than the Al-TiAl critical temperature. The copper holder was closed and covered by aluminum foil to mitigate environmental radiation. Finally, a mu-metal shield was placed outside the cryostat to reduce magnetic-field effects<sup>47</sup>.

To calibrate the detectors and characterize their pulses, three optical fibers were placed facing the side of the silicon tile opposite to the KIDs: two positioned to face

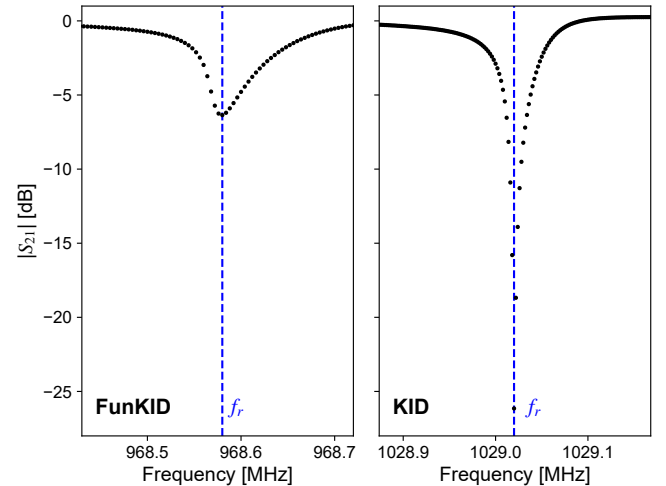


FIG. 4: Transmission function amplitude  $|S_{21}|$  around the resonance frequencies  $f_r$  of the resonators.

the center of each resonator, and one located midway between them. The two lateral fibers were used to identify the two pixels, while the central one was used to calibrate the KIDs from the same position for comparison. The fibers were pulsed with 400 nm photons bursts generated at room temperature by controlled a LED lamp<sup>48</sup>.

The readout tones were generated by the NIXA electronic system<sup>49,50</sup>, a superheterodyne radio-frequency detection system capable to transmit and receive tones at the KIDs resonant frequencies. The transmitted waves undergo an attenuation chain of 55 dB before the chip, are transmitted past the resonators, then are amplified by 30 dB by a Low Noise Amplifier (model: CITLF3<sup>51</sup>) operated at 4 K and finally received back by NIXA.

The resonances of the two KIDs are shown in Fig. 4. We fitted both the amplitude of the transmission function  $|S_{21}|$  and its real and imaginary components in order to extract the resonant frequencies of the two KIDs as well as the quality factors  $Q_c$ ,  $Q_i$ , and  $Q$ . We also evaluated the resonator ring times  $\tau_{\text{ring}} = Q/\pi f_r$  of the two KIDs. The results are reported in Tab. I.

A shift of around -40 MHz of the measured FunKID resonant frequency with respect to the simulation was observed, indicating that the overlap regions between the funnels and the resonator might have not been correctly modeled in the simulations. Conversely, the obtained KID resonant frequency is in agreement with sim-

	$f_r$ [MHz]	$Q_c$ [k]	$Q_i$ [k]	$Q$ [k]	$\tau_{\text{ring}}$ [ $\mu\text{s}$ ]
<b>FunKID</b>	968.6	19	20	10	3
<b>KID</b>	1029.0	20	410	19	6

TABLE I: Results of the resonant frequency  $f_r$ , quality factors  $Q$ ,  $Q_i$  and  $Q_c$  and ring times  $\tau_{\text{ring}}$  of the two resonators. The uncertainty of the resonant frequency is negligible, while the relative uncertainty on the internal quality factor  $Q_i$  was estimated to around 10 %.

ulation, assuming a kinetic inductance  $L_k = 1.4 \text{ pH/sq}$ , which is the same of Ref.<sup>33</sup>. The coupling quality factors  $Q_c \sim 20 \text{ k}$  are in line with the values simulated with SONNET, for both resonators. In addition, the internal quality factor of the FunKID is comparable to the coupling quality factor, which currently limits this design. Conversely, the internal quality of the KID is higher than the FunKID and in line with the values obtained in Ref.<sup>33</sup>, indicating that the reduced  $Q_i$  of the FunKID is set by the funnels and not by fabrication processes of the trilayer AlTiAl film.

For each resonator, we evaluated our best estimate of kinetic inductance fraction  $\alpha$ , by combining the measured resonant frequencies  $f_r$  with the resonant frequencies  $f_0$  obtained from SONNET simulations performed with a perfect conductor (i.e., with  $L_k = 0$ ), through the formula:

$$\alpha = 1 - \left( \frac{f_r}{f_0} \right)^2 \quad (5)$$

The simulations were calibrated against two identical resonators but in Aluminum. We obtained  $\alpha = 18.9\%$  and  $\alpha = 15.6\%$  for the FunKID and the KID, respectively, much larger than those obtained in Aluminum,  $\alpha = 7.0\%$  and  $\alpha = 5.0\%$  using the same design, consistently with an increase of kinetic inductance  $L_k$ <sup>33</sup>.

We also measured the feed-line critical temperature  $T_c = (0.83 \pm 0.08) \text{ K}$ , corresponding to a superconducting gap  $\Delta_0 = (125.9 \pm 12.6) \mu\text{eV}$ , and we assumed that this coincided with the critical temperature of the normal KID. Such value is in reasonable agreement with that found by the CALDER project<sup>33</sup> of 0.81 K, using a similar film. Nevertheless such estimation is reliable as long as it is applied to the normal KID. The presence of funnels is expected to modify the FunKID critical temperature, but in the current setup we do not have a direct way to measure it.

We also measured  $\delta f_r/f_r$ , the relative shift of the resonant frequency with respect to the base temperature resonant frequency,  $f_r$ . Using a model based on the BCS theory<sup>27</sup>, it is possible to write:

$$\frac{\delta f_r}{f_r} = -\frac{\alpha}{2} S_2(f_r, T) \sqrt{\frac{2\pi k_B T}{\Delta(T)}} e^{-\Delta(T)/k_B T} \quad (6)$$

where  $\Delta(T)$  is the AlTiAl superconducting order parameter<sup>27</sup>. For this purpose, we measured the resonant frequency of each resonator at different temperatures, while keeping the transmission bias powers fixed at  $-87 \text{ dBm}$  and  $-71 \text{ dBm}$  for the FunKID and the KID, respectively. These powers are lower than the operative calibration powers in order to isolate the effect of thermally generated excess QPs in the resonators, while keeping the micro-wave induced contribution as low as possible<sup>52</sup>. However, potential limitations may arise when applying such a model to inhomogeneous and multilayer superconductors. In order to test the applicability of such model to our devices, we compared the data with the BCS model

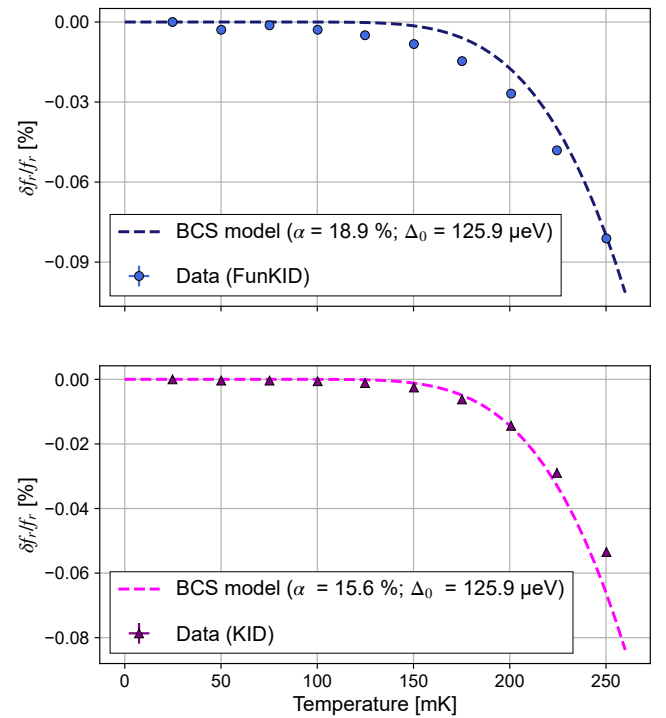


FIG. 5: Relative shift of the resonant frequency with respect to the base temperature resonant frequency,  $\delta f_r/f_r$ , for the FunKID in blue and KID in purple. The dashed curves are obtained with the BCS model calculated with our best predictions of  $\alpha$  and  $\Delta_0$ .

calculated with our best predictions of  $\alpha$  and  $\Delta_0$  (Fig. 5).

In both cases, data deviate from the BCS model. The FunKID shows significant discrepancies at intermediate temperatures, indicating that the presence of the funnels and the trilayer KID structure prevents the BCS model from fully describing the device. For the normal KID, the overall behavior of data is similar to the BCS model, although deviations at high temperatures are still observed. Therefore more complete models than the BCS-based one would be required for a more accurate interpretation<sup>35</sup>, but these are beyond the scope of this work.

To calibrate the detectors, the FunKID and the KID were operated at bias transmission calibration powers  $P_{\text{cal}}$  of  $-68 \text{ dBm}$  and  $-62 \text{ dBm}$ , respectively, at which they exhibited good performance in terms of signal to noise ratio<sup>33</sup>. The choice to operate the FunKID with a lower calibration power was motivated by the observation that on the FunKID non-linear effects became relevant at smaller power than the KID<sup>23</sup>. Optical pulses of increasing total energy from  $\sim 9 \text{ keV}$  up to  $\sim 90 \text{ keV}$  were fired onto the back of the substrate by means of the central fiber to characterize the response of the two KIDs<sup>48</sup>. Finally, the signals were processed offline with a matched filter<sup>53</sup> in order to further improve the signal to noise ratio.

Two pulses generated by an energy release of around  $90 \text{ keV}$  into the substrate have been superimposed in

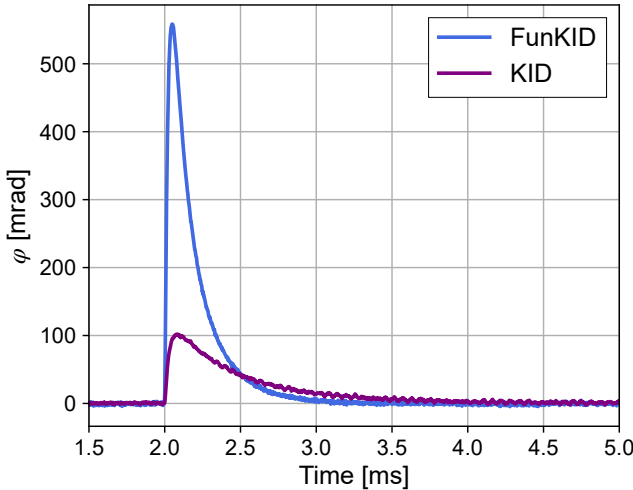


FIG. 6: Two pulses generated by the same energy release. A higher response is observed for the FunKID resonator compared to the normal KID. Also, it is possible to notice the higher  $\tau_d$  of the KID pulse, which takes almost 2 ms to come back to the baseline level.

Fig. 6. It is possible to observe that the FunKID exhibits a pulse response about 5.5 times higher than the KID. Our best prediction for the gain in responsivity under identical electrical conditions was around 8. According to Eq. 4 the dominant degradation of the FunKID response might be associated with its smaller quality factor  $Q$ , which is a factor 1.9 lower than that of the KID. However, our best prediction of  $\alpha$  of the FunKID is about 1.2 higher than that of the KID. By correcting the best gain prediction with these two effects, we obtain a gain of around 5.1, similar to measurements.

The decay times  $\tau_d$  of the FunKID and KID are about 0.15 ms and 0.45 ms, respectively. The longer decay time of the KID is in line with the higher internal quality factor<sup>54</sup>. The rise times  $\tau_{\text{rise}}$  amount to around 12  $\mu$ s and 20  $\mu$ s, respectively. These are significantly higher than the respective ring times (see Tab I). In addition, the rise time of the FunKID is higher than the QPs diffusion time scale  $\tau_{\text{diff}} \simeq 4 \mu\text{s}$  previously defined. It seems reasonable that in both cases the rise times of the pulses are dominated by the phonon absorption time  $\tau_{\text{ph}}$ <sup>17,28</sup>, which can be faster in the case of the FunKID due to its higher phonon collection efficiency.

The results of the energy calibrations<sup>25,33,48</sup> of the two KIDs, the phase responsivity  $r$ , the noise RMS after applying the matched filter,  $\sigma_N$ , and the corresponding baseline energy resolution of the device,  $\sigma_E$ , have been reported in Tab. II. The phase responsivity is about 5.3 higher at the calibration power for the FunKID, which is in line with the measured responsivity gain previously discussed. Moreover, an improvement of around a factor of 2 for the energy resolution in eV is measured, despite the worse noise RMS  $\sigma_N$  of the FunKID. The improvement of the FunKID responsivity was therefore proven,

	<b>FunKID</b>	<b>KID</b>
$P_{\text{cal}}$ [dBm]	-68	-62
$r$ [mrad/keV]	$5.85 \pm 0.14$	$1.11 \pm 0.04$
$\sigma_N$ [mrad]	$0.386 \pm 0.009$	$0.173 \pm 0.005$
$\sigma_E$ [eV]	$65.9 \pm 2.3$	$156 \pm 6$

TABLE II: Results of the energy calibrations performed on the two KIDs. For each device, we report the calibration power  $P_{\text{cal}}$ , the phase responsivity  $r$ , the noise RMS after the matched filter  $\sigma_N$  and energy resolution  $\sigma_E$ .

even with a total quality factor smaller by a factor of about 2.

While the tested device served as a proof of concept and the improvement in detector responsivity was demonstrated, an enhancement in energy resolution is still required, as the current performance remains worse than previously achieved results<sup>14</sup>. Achieving this improvement will demand further optimization, such as an additional increase of the total quality factors  $Q$ , which in turn requires higher internal quality factors  $Q_i$ .

## ACKNOWLEDGMENTS

This work was supported by the INFN, Sapienza University of Rome and co-funded by the European Union (ERC, DANAЕ, 101087663). Views and opinions expressed are however those of the author(s) only and do not necessarily reflect those of the European Union or the European Research Council. Neither the European Union nor the granting authority can be held responsible for them. We thank A. Girardi and M. Iannone of the INFN Sezione di Roma for technical support. We acknowledge the support of the PTA platform for the fabrication of the device.

## AUTHOR DECLARATIONS

### Conflict of Interest

The authors have no conflicts to disclose.

## DATA AVAILABILITY STATEMENT

The data that support the findings of this study are available from the corresponding author upon reasonable request.

<sup>1</sup>A. H. Abdelhameed, G. Angloher, P. Bauer, A. Bento, E. Bertoldo, C. Bucci, L. Canonica, A. D'Addabbo, X. Defay, S. Di Lorenzo, A. Erb, F. v. Feilitzsch, S. Fichtinger, N. Ferreiro Iachellini, A. Fuss, P. Gorla, D. Hauff, J. Jochum, A. Kinast, H. Kluck, H. Kraus, A. Langenkämper, M. Mancuso, V. Mokina, E. Mondragon, A. Münster, M. Olmi, T. Ortmann, C. Pagliarone, L. Pattavina, F. Petricca, W. Pottzel,

F. Pröbst, F. Reindl, J. Rothe, K. Schäffner, J. Schieck, V. Schipperges, D. Schmiedmayer, S. Schönert, C. Schwertner, M. Stahlberg, L. Stodolsky, C. Strandhagen, R. Strauss, C. Türkoglu, I. Usherov, M. Willers, and V. Zema (CRESST Collaboration), “First results from the CRESST-III low-mass dark matter program,” *Phys. Rev. D* **100**, 102002 (2019).

<sup>2</sup>E. Armengaud, Q. Arnaud, C. Augier, A. Benoît, A. Benoît, L. Bergé, T. Bergmann, J. Billard, J. Blümner, T. de Boissière, G. Bres, A. Broniatowski, V. Brudanin, P. Camus, A. Cazes, M. Chapellier, F. Charlieux, L. Dumoulin, K. Eitel, D. Filosov, N. Foerster, N. Fourches, G. Garde, J. Gascon, G. Gerbier, A. Giuliani, M. Grollier, M. Gros, L. Hehn, S. Hervé, G. Heuermann, V. Humbert, M. D. Jésus, Y. Jin, S. Jokisch, A. Juillard, C. Kéfélian, M. Kleifges, V. Kozlov, H. Kraus, V. Kudryavtsev, H. Le-Sueur, J. Lin, M. Mancuso, S. Marnieros, A. Menshikov, X.-F. Navick, C. Nones, E. Olivieri, P. Pari, B. Paul, M.-C. Piro, D. Poda, E. Queguiner, M. Robinson, H. Rodeinas, S. Rozov, V. Sanglard, B. Schmidt, S. Scorza, B. Siebenborn, D. Tcherniakhovski, L. Vagneron, M. Weber, E. Yakeshev, and X. Zhang, “Constraints on low-mass WIMPs from the EDELWEISS-III dark matter search,” *Nature* **536**, 019 (2016).

<sup>3</sup>R. Agnese, T. Aramaki, I. J. Arnquist, W. Baker, D. Balakishiyeva, S. Banik, D. Barker, R. Basu Thakur, D. A. Bauer, T. Binder, M. A. Bowles, P. L. Brink, R. Bunker, B. Cabrera, D. O. Caldwell, R. Calkins, C. Cartaro, D. G. Cerdeño, Y. Chang, Y. Chen, J. Cooley, B. Cornell, P. C. F. Di Stefano, T. Doughty, E. Fascione, E. Figueroa-Feliciano, M. Fritts, G. Gerbier, R. Germond, M. Ghaith, G. L. Godfrey, S. R. Golwala, J. Hall, H. R. Harris, Z. Hong, E. W. Hoppe, L. Hsu, M. E. Huber, V. Iyer, D. Jardin, A. Jastram, C. Jena, M. H. Kelsey, A. Kennedy, A. Kubik, N. A. Kurinsky, B. Loer, E. Lopez Asamar, P. Lukens, D. MacDonell, R. Mahapatra, V. Mandic, N. Mast, E. H. Miller, N. Mirabolfathi, B. Mohanty, J. D. Morales Mendoza, J. Nelson, J. L. Orrell, S. M. Oser, K. Page, W. A. Page, R. Partridge, M. Penalver Martinez, M. Pepin, A. Phipps, S. Poudel, M. Pyle, H. Qiu, W. Rau, P. Redl, A. Reisetter, T. Reynolds, A. Roberts, A. E. Robinson, H. E. Rogers, T. Saab, B. Sadoulet, J. Sander, K. Schneck, R. W. Schnee, S. Scorza, K. Senapati, B. Serfass, D. Speller, M. Stein, J. Street, H. A. Tanaka, D. Toback, R. Underwood, A. N. Villano, B. von Krosigk, B. Welliver, J. S. Wilson, M. J. Wilson, D. H. Wright, S. Yellin, J. J. Yen, B. A. Young, X. Zhang, and X. Zhao (SuperCDMS Collaboration), “Results from the Super Cryogenic Dark Matter Search Experiment at Soudan,” *Phys. Rev. Lett.* **120**, 061802 (2018).

<sup>4</sup>R. Strauss, J. Rothe, G. Angloher, A. Bento, A. Gütlein, D. Hauff, H. Kluck, M. Mancuso, L. Oberauer, F. Petricca, F. Pröbst, J. Schieck, S. Schönert, W. Seidel, and L. Stodolsky, “Gram-scale cryogenic calorimeters for rare-event searches,” *Phys. Rev. D* **96**, 022009 (2017).

<sup>5</sup>J. Billard, R. Carr, J. Dawson, E. Figueroa-Feliciano, J. A. Formaggio, J. Gascon, S. T. Heine, M. De Jesus, J. Johnston, T. Lasserre, A. Leder, K. J. Palladino, V. Sibille, M. Vivier, and L. Winslow, “Coherent neutrino scattering with low temperature bolometers at Chooz reactor complex,” *Journal of Physics G: Nuclear and Particle Physics* **44**, 105101 (2017).

<sup>6</sup>C. Augier, G. Beaulieu, V. Belov, L. Berge, J. Billard, G. Bres, J.-L. Bret, A. Broniatowski, M. Calvo, A. Cazes, D. Chaize, M. Chapellier, L. Chaplinsky, G. Chemin, R. Chen, J. Colas, M. de Jesus, P. de Marcillac, L. Dumoulin, O. Exshaw, S. Ferriol, E. Figueroa-Feliciano, J.-B. Filippini, J. A. Formaggio, S. Fuard, J. Gascon, A. Giuliani, J. Goupy, C. Goy, C. Guerin, C. F. Hirschbèghin, P. Harrington, S. T. Heine, S. A. Hertel, M. Heusch, C. Hoarau, Z. Hong, J.-C. Ianigro, Y. Jin, J. P. Johnston, A. Juillard, S. Kazarcev, J. Lamblin, H. Lattaud, A. Lubashevskiy, D. W. Mayer, S. Marnieros, J. Minet, D. Misiak, A. Monfardini, F. Mounier, E. Olivieri, C. Oriol, P. K. Patel, E. Perbet, H. D. Pinckney, D. Ponomarev, D. Poda, F. Rarbi, J.-S. Real, J.-S. Ricol, T. Redon, A. Robert, S. Rozov, I. Rozova, T. Salagnac, V. Sanglard, B. Schmidt, Y. Shevchik, V. Sibille, T. Soldner, J. Stachurska, A. Stutz, L. Vagneron, W. van de Pontseele, F. Vezzu, S. Weber, L. Winslow, E. Yakeshev, and D. Zinatulina, “Ricochet Progress and Status,” *Journal of Low Temperature Physics* **212**, 127–137 (2023).

<sup>7</sup>G. Agnolet, W. Baker, D. Barker, R. Beck, T. Carroll, J. Cesari, P. Cushman, J. Dent, S. De Rijck, B. Dutta, W. Flanagan, M. Fritts, Y. Gao, H. Harris, C. Hays, V. Iyer, A. Jastram, F. Kadribasic, A. Kennedy, A. Kubik, K. Lang, R. Mahapatra, V. Mandic, C. Marianno, R. Martin, N. Mast, S. McDeavitt, N. Mirabolfathi, B. Mohanty, K. Nakajima, J. Newhouse, J. Newstead, I. Ogawa, D. Phan, M. Proga, A. Rajput, A. Roberts, G. Rogachev, R. Salazar, J. Sander, K. Senapati, M. Shimada, B. Soubasis, L. Strigari, Y. Tamagawa, W. Teizer, J. Vermaak, A. Villano, J. Walker, B. Webb, Z. Wetzel, and S. Yadavalli, “Background studies for the MINER Coherent Neutrino Scattering reactor experiment,” *Nuclear Instruments and Methods in Physics Research Section A: Accelerators, Spectrometers, Detectors and Associated Equipment* **853**, 53–60 (2017).

<sup>8</sup>D. Akimov, J. B. Albert, P. An, C. Awe, P. S. Barbeau, B. Becker, V. Belov, A. Brown, A. Bolozdynya, B. Cabrera-Palmer, M. Cervantes, J. I. Collar, R. J. Cooper, R. L. Cooper, C. Cuesta, D. J. Dean, J. A. Detwiler, A. Eberhardt, Y. Efremenko, S. R. Elliott, E. M. Erkela, L. Fabris, M. Febbraro, N. E. Fields, W. Fox, Z. Fu, A. Galindo-Uribarri, M. P. Green, M. Hai, M. R. Heath, S. Hedges, D. Hornback, T. W. Hossbach, E. B. Iverson, L. J. Kaufman, S. Ki, S. R. Klein, A. Khromov, A. Konovalov, M. Kremer, A. Kumpan, C. Leadbetter, L. Li, W. Lu, K. Mann, D. M. Markoff, K. Miller, H. Moreno, P. E. Mueller, J. Newby, J. L. Orrell, C. T. Overman, D. S. Parno, S. Penttila, G. Perumpilly, H. Ray, J. Raybern, D. Reyna, G. C. Rich, D. Rimal, D. Rudik, K. Scholberg, B. J. Scholz, G. Sinev, W. M. Snow, V. Sosnovtsev, A. Shakirov, S. Suchyta, B. Suh, R. Tayloe, R. T. Thornton, I. Tolstukhin, J. Vanderwerp, R. L. Varner, C. J. Virtue, Z. Wan, J. Yoo, C.-H. Yu, A. Zawada, J. Zettlemoyer, A. M. Zderic, and C. Collaboration, “Observation of coherent elastic neutrino-nucleus scattering,” *Science* **357**, 1123–1126 (2017).

<sup>9</sup>I. Alkhateb, D. W. P. Amaral, T. Aralis, T. Aramaki, I. J. Arnquist, I. Ataee Langroudy, E. Azadbakht, S. Banik, D. Barker, C. Bathurst, D. A. Bauer, L. V. S. Bezerra, R. Bhattacharyya, T. Binder, M. A. Bowles, P. L. Brink, R. Bunker, B. Cabrera, R. Calkins, R. A. Cameron, C. Cartaro, D. G. Cerdeño, Y.-Y. Chang, M. Chaudhuri, R. Chen, N. Chott, J. Cooley, H. Coombes, J. Corbett, P. Cushman, F. De Brienne, M. L. di Vacri, M. D. Diamond, E. Fascione, E. Figueroa-Feliciano, C. W. Fink, K. Fouts, M. Fritts, G. Gerbier, R. Germond, M. Ghaith, S. R. Golwala, H. R. Harris, N. Herbert, B. A. Hines, M. I. Hollister, Z. Hong, E. W. Hoppe, L. Hsu, M. E. Huber, V. Iyer, D. Jardin, A. Jastram, V. K. S. Kashyap, M. H. Kelsey, A. Kubik, N. A. Kurinsky, R. E. Lawrence, A. Li, B. Loer, E. Lopez Asamar, P. Lukens, D. MacDonell, D. B. MacFarlane, R. Mahapatra, V. Mandic, N. Mast, A. J. Mayer, H. Meyer zu Theenhausen, E. M. Michaud, E. Michelin, N. Mirabolfathi, B. Mohanty, J. D. Morales Mendoza, S. Nagorny, J. Nelson, H. Neog, V. Novati, J. L. Orrell, S. M. Oser, W. A. Page, P. Pakarha, R. Partridge, R. Podvianik, F. Ponce, S. Poudel, M. Pyle, W. Rau, E. Reid, R. Ren, T. Reynolds, A. Roberts, A. E. Robinson, T. Saab, B. Sadoulet, J. Sander, A. Sattari, R. W. Schnee, S. Scorza, B. Serfass, D. J. Sincavage, C. Stanford, J. Street, D. Toback, R. Underwood, S. Verma, A. N. Villano, B. von Krosigk, S. L. Watkins, L. Wills, J. S. Wilson, M. J. Wilson, J. Winchell, D. H. Wright, S. Yellin, B. A. Young, T. C. Yu, E. Zhang, H. G. Zhang, X. Zhao, L. Zheng, J. Camilleri, Y. G. Kolomensky, and S. Zuber (SuperCDMS Collaboration), “Light Dark Matter Search with a High-Resolution Athermal Phonon Detector Operated above Ground,” *Phys. Rev. Lett.* **127**, 061801 (2021).

<sup>10</sup>R. Anthony-Petersen, C. L. Chang, Y.-Y. Chang, L. Chaplinsky, C. W. Fink, M. Garcia-Sciveres, W. Guo, S. A. Hertel, X. Li, J. Lin, M. Lisovenko, R. Mahapatra, W. Matava, D. N. McKinsey, D. Z. Osterman, P. K. Patel, B. Penning, M. Platt, M. Pyle,

Y. Qi, M. Reed, I. Rydstrom, R. K. Romani, B. Sadoulet, B. Serrfass, P. Sorensen, B. Suerfu, V. Velan, G. Wang, Y. Wang, S. L. Watkins, and M. R. Williams, "Low energy backgrounds and excess noise in a two-channel low-threshold calorimeter," *Applied Physics Letters* **126**, 102601 (2025).

<sup>11</sup>E. Armengaud, C. Augier, A. Benoît, A. Benoit, L. Bergé, J. Billard, A. Broniatowski, P. Camus, A. Cazes, M. Chapellier, F. Charlieux, D. Ducimetière, L. Dumoulin, K. Eitel, D. Filosofov, J. Gascon, A. Giuliani, M. Gros, M. De Jésus, Y. Jin, A. Juillard, M. Kleifges, R. Maisonneuve, S. Marnieros, D. Misiak, X.-F. Navick, C. Nones, E. Olivieri, C. Oriol, P. Pari, B. Paul, D. Poda, E. Queguiner, S. Rozov, V. Sanglard, B. Siebenborn, L. Vagneron, M. Weber, E. Yakushev, A. Zolotarova, and B. J. Kavanagh (EDELWEISS Collaboration), "Searching for low-mass dark matter particles with a massive Ge bolometer operated above ground," *Phys. Rev. D* **99**, 082003 (2019).

<sup>12</sup>A. Cruciani, L. Bandiera, M. Calvo, N. Casali, I. Colantoni, G. Del Castello, M. del Gallo Roccagiovine, D. Delicato, M. Giammie, V. Guidi, J. Goupy, V. Pettinacci, G. Pettinari, M. Romagnoni, M. Tamisari, A. Mazzolari, A. Monfardini, and M. Vignati, "BULLKID: Monolithic array of particle absorbers sensed by kinetic inductance detectors," *Applied Physics Letters* **121**, 213504 (2022).

<sup>13</sup>P. K. Day, H. G. LeDuc, B. A. Mazin, A. Vayonakis, and J. Zmuidzinas, "A broadband superconducting detector suitable for use in large arrays," *Nature* **425**, 817–821 (2003).

<sup>14</sup>D. Delicato, A. Ahmad, L. Bandiera, M. Calvo, M. Cappelli, G. Del Castello, M. del Gallo Roccagiovine, M. Giammie, V. Guidi, D. Maiello, V. Pettinacci, M. Romagnoni, M. Tamisari, A. Cruciani, A. Mazzolari, A. Monfardini, and M. Vignati, "Low-energy spectrum of the BULLKID detector array operated on surface," *The European Physical Journal C* **84**, 353 (2024).

<sup>15</sup>B. A. Mazin, J. Bailey, J. Bartlett, C. Bockstiegel, B. Bumble, G. Coiffard, T. Currie, M. Daal, K. Davis, R. Dodkins, N. Fruhwala, N. Jovanovic, I. Lipartito, J. Lozi, J. Males, D. Mawet, S. Meeker, K. O'Brien, M. Rich, J. Smith, S. Steiger, N. Swimmer, A. Walter, N. Zobrist, and J. Zmuidzinas, "Optical and Near-IR Microwave Kinetic Inductance Detectors (MKIDs) in the 2020s," (2019), arXiv:1908.02775 [astro-ph.IM].

<sup>16</sup>Adam, R., Adane, A., Ade, P. A. R., André, P., Andrianasolo, A., Aussel, H., Beelen, A., Benoît, A., Bideaud, A., Billot, N., Bourrion, O., Bracco, A., Calvo, M., Catalano, A., Coiffard, G., Comis, B., De Petris, M., Désert, F.-X., Doyle, S., Driessen, E. F. C., Evans, R., Goupy, J., Kramer, C., Lagache, G., Leclercq, S., Leggeri, J.-P., Lestrade, J.-F., Macías-Pérez, J. F., Mauskopf, P., Mayet, F., Maury, A., Monfardini, A., Navarro, S., Pascale, E., Perotto, L., Pisano, G., Ponthieu, N., Revéret, V., Rigby, A., Ritacco, A., Romero, C., Roussel, H., Ruppin, F., Schuster, K., Sievers, A., Triqueneaux, S., Tucker, C., and Zylka, R., "The NIKA2 large-field-of-view millimetre continuum camera for the 30 m IRAM telescope," *A&A* **609**, A115 (2018).

<sup>17</sup>L. J. Swenson, A. Cruciani, A. Benoit, M. Roesch, C. S. Yung, A. Bideaud, and A. Monfardini, "High-speed phonon imaging using frequency-multiplexed kinetic inductance detectors," *Applied Physics Letters* **96**, 263511 (2010).

<sup>18</sup>A. Cruciani, L. J. Swenson, A. Monfardini, N. Boudou, M. Calvo, and M. Roesch, "X-Ray Imaging Using LEKIDs," *Journal of Low Temperature Physics* **167**, 311–317 (2012).

<sup>19</sup>S. Golwala, J. Gao, D. Moore, B. Mazin, M. Eckart, B. Bumble, P. Day, H. G. LeDuc, and J. Zmuidzinas, "A WIMP Dark Matter Detector Using MKIDs," *Journal of Low Temperature Physics* **151**, 550–556 (2008).

<sup>20</sup>J. Zmuidzinas, "Superconducting Microresonators: Physics and Applications," *Annual Review of Condensed Matter Physics* **3**, 169–214 (2012).

<sup>21</sup>B. A. Mazin, *Microwave Kinetic Inductance Detectors*, Phd thesis, California Institute of Technology (2005).

<sup>22</sup>M. S. Khalil, M. J. A. Stoutimore, F. C. Wellstood, and K. D. Osborn, "An analysis method for asymmetric resonator transmission applied to superconducting devices," *Journal of Applied Physics* **90**, 355–364 (2001).

<sup>23</sup>L. J. Swenson, P. K. Day, B. H. Eom, H. G. Leduc, N. Llombart, C. M. McKenney, O. Noroozian, and J. Zmuidzinas, "Operation of a titanium nitride superconducting microresonator detector in the nonlinear regime," *Journal of Applied Physics* **113**, 104501 (2013).

<sup>24</sup>M. Vignati, C. Bellenghi, L. Cardani, N. Casali, I. Colantoni, and A. Cruciani, "Non-linearity in the system of quasiparticles of a superconducting resonator," (2021), arXiv:2102.09431 [cond-mat.supr-con].

<sup>25</sup>D. Delicato, D. Angelone, L. Bandiera, M. Calvo, M. Cappelli, U. Chowdhury, G. Del Castello, M. Folcarelli, M. del Gallo Roccagiovine, V. Guidi, G. L. Pesce, M. Romagnoni, A. Cruciani, A. Mazzolari, A. Monfardini, and M. Vignati, "Germanium target sensed by phonon-mediated kinetic inductance detectors," *Applied Physics Letters* **126**, 153502 (2025).

<sup>26</sup>D. C. Moore, S. R. Golwala, B. Bumble, B. Cornell, P. K. Day, H. G. LeDuc, and J. Zmuidzinas, "Position and energy-resolved particle detection using phonon-mediated microwave kinetic inductance detectors," *Applied Physics Letters* **100**, 232601 (2012).

<sup>27</sup>J. Gao, J. Zmuidzinas, A. Vayonakis, P. Day, B. Mazin, and H. Leduc, "Equivalence of the Effects on the Complex Conductivity of Superconductor due to Temperature Change and External Pair Breaking," *Journal of Low Temperature Physics* **151**, 557–563 (2008).

<sup>28</sup>M. Martinez, L. Cardani, N. Casali, A. Cruciani, G. Pettinari, and M. Vignati, "Measurements and Simulations of Athermal Phonon Transmission from Silicon Absorbers to Aluminum Sensors," *Phys. Rev. Appl.* **11**, 064025 (2019).

<sup>29</sup>A. Fyhrie, C. McKenney, J. Glenn, H. G. LeDuc, J. Gao, P. Day, and J. Zmuidzinas, "Responsivity boosting in FIR TiN LEKIDs using phonon recycling: simulations and array design," in *Millimeter, Submillimeter, and Far-Infrared Detectors and Instrumentation for Astronomy VIII*, Vol. 9914 (SPIE, 2016) pp. 570–576.

<sup>30</sup>A. L. D. Santis, *Phonon mediated kinetic inductance detector with phonon funneling volume*, Master's thesis, Sapienza Università di Roma (2022).

<sup>31</sup>B. A. Mazin, B. Bumble, P. K. Day, M. E. Eckart, S. Golwala, J. Zmuidzinas, and F. A. Harrison, "Position sensitive x-ray spectrophotometer using microwave kinetic inductance detectors," *Applied Physics Letters* **89**, 222507 (2006).

<sup>32</sup>L. Pesce, M. Calvo, M. Cappelli, U. Chowdhury, A. L. De Santis, G. Del Castello, D. Delicato, M. Folcarelli, M. del Gallo Roccagiovine, D. Quaranta, A. Cruciani, A. Monfardini, and M. Vignati, "Preliminary tests of a phonon-mediated Kinetic Inductance Detector with phonon-funneling volume," in *Proceedings of the IFAE 2025 Conference* (Società Italiana di Fisica, Bologna, 2026).

<sup>33</sup>L. Cardani, N. Casali, A. Cruciani, H. I. Sueur, M. Martinez, F. Bellini, M. Calvo, M. G. Castellano, I. Colantoni, C. Cosmelli, A. D'Addabbo, S. D. Domizio, J. Goupy, L. Minutolo, A. Monfardini, and M. Vignati, "Al/Ti/Al phonon-mediated KIDs for UV–vis light detection over large areas," *Superconductor Science and Technology* **31**, 075002 (2018).

<sup>34</sup>Catalano, A., Goupy, J., le Sueur, H., Benoit, A., Bourrion, O., Calvo, M., D'Addabbo, A., Dumoulin, L., Levy-Bertrand, F., Macías-Pérez, J., Marnieros, S., Ponthieu, N., and Monfardini, A., "Bi-layer kinetic inductance detectors for space observations between 80–120 GHz," *A&A* **580**, A15 (2015).

<sup>35</sup>S. Zhao, D. J. Goldie, S. Withington, and C. N. Thomas, "Exploring the performance of thin-film superconducting multilayers as kinetic inductance detectors for low-frequency detection," *Superconductor Science and Technology* **31**, 015007 (2017).

<sup>36</sup>G. Brammertz, A. Poelaert, A. A. Golubov, P. Verhoeve, A. Peacock, and H. Rogalla, "Generalized proximity effect model in superconducting bi- and trilayer films," *Journal of Applied Physics* **90**, 355–364 (2001).

<sup>37</sup>S. Zhao, D. J. Goldie, C. N. Thomas, and S. Withington, "Calculation and measurement of critical temperature in thin super-

conducting multilayers,” *Superconductor Science and Technology* **31**, 105004 (2018).

<sup>38</sup>L. Cardani, N. Casali, I. Colantoni, A. Cruciani, S. Di Domizio, M. Martinez, V. Pettinacci, G. Pettinari, and M. Vignati, “Final results of CALDER: kinetic inductance light detectors to search for rare events,” *The European Physical Journal C* **81**, 636 (2021).

<sup>39</sup>R.-P. Riwar and G. Catelani, “Efficient quasiparticle traps with low dissipation through gap engineering,” *Phys. Rev. B* **100**, 144514 (2019).

<sup>40</sup>T. Nussbaumer, P. Lerch, E. Kirk, A. Zehnder, R. Füchsli, P. F. Meier, and H. R. Ott, “Quasiparticle diffusion in tantalum using superconducting tunnel junctions,” *Phys. Rev. B* **61**, 9719–9728 (2000).

<sup>41</sup>S. Y. Hsieh and J. L. Levine, “Diffusion of Quasiparticles in Superconducting Aluminum Films,” *Phys. Rev. Lett.* **20**, 1502–1504 (1968).

<sup>42</sup>M. Zgirski, M. Foltyn, A. Savin, A. Naumov, and K. Norowski, “Heat Hunting in a Freezer: Direct Measurement of Quasiparticle Diffusion in Superconducting Nanowire,” *Phys. Rev. Appl.* **14**, 044024 (2020).

<sup>43</sup>P. J. de Visser, J. J. A. Baselmans, P. Diener, S. J. C. Yates, A. Endo, and T. M. Klapwijk, “Number Fluctuations of Sparse Quasiparticles in a Superconductor,” *Phys. Rev. Lett.* **106**, 167004 (2011).

<sup>44</sup>R. Barends, J. J. A. Baselmans, S. J. C. Yates, J. R. Gao, J. N. Hovenier, and T. M. Klapwijk, “Quasiparticle Relaxation in Optically Excited High-*Q* Superconducting Resonators,” *Phys. Rev. Lett.* **100**, 257002 (2008).

<sup>45</sup>Sonnet Software, “Sonnet Software Website,” <https://www.sonnetsoftware.com/>, accessed: 2025-07-29.

<sup>46</sup>Plateforme technologique amont, “Our Facilities Overview,” <http://pta-grenoble.com/our-facilities/overview>, accessed: 2025-07-29.

<sup>47</sup>D. Flanigan, B. R. Johnson, M. H. Abitbol, S. Bryan, R. Cantor, P. Day, G. Jones, P. Mauskopf, H. McCarrick, A. Miller, and J. Zmuidzinas, “Magnetic field dependence of the internal quality factor and noise performance of lumped-element kinetic inductance detectors,” *Applied Physics Letters* **109**, 143503 (2016).

<sup>48</sup>G. Del Castello, “LANTERN: A multichannel light calibration system for cryogenic detectors,” *Nuclear Instruments and Methods in Physics Research Section A: Accelerators, Spectrometers, Detectors and Associated Equipment* **1068**, 169728 (2024).

<sup>49</sup>O. Bourrion, A. Bideaud, A. Benoit, A. Cruciani, J. F. Macias-Perez, A. Monfardini, M. Roesch, L. Swenson, and C. Vescovi, “Electronics and data acquisition demonstrator for a kinetic inductance camera,” *Journal of Instrumentation* **6**, P06012 (2011).

<sup>50</sup>O. Bourrion, C. Vescovi, A. Catalano, M. Calvo, A. D’Addabbo, J. Goupy, N. Boudou, J. F. Macias-Perez, and A. Monfardini, “High speed readout electronics development for frequency-multiplexed kinetic inductance detector design optimization,” *Journal of Instrumentation* **8**, C12006 (2013).

<sup>51</sup>Cosmic Microwave Technology, Inc., “Citrif3 low noise amplifier datasheet,” <https://www.everythingrf.com/products/microwave-rf-amplifiers/cosmic-microwave-technology-inc/567-1897-citrif3> (2025), datasheet available at EverythingRF.

<sup>52</sup>P. J. de Visser, J. J. A. Baselmans, S. J. C. Yates, P. Diener, A. Endo, and T. M. Klapwijk, “Microwave-induced excess quasiparticles in superconducting resonators measured through correlated conductivity fluctuations,” *Applied Physics Letters* **100**, 162601 (2012).

<sup>53</sup>E. Gatti and P. F. Manfredi, “Processing the signals from solid-state detectors in elementary-particle physics,” *La Rivista del Nuovo Cimento (1978-1999)* **9**, 1–146 (1986).

<sup>54</sup>A. Cruciani, F. Bellini, L. Cardani, N. Casali, M. G. Castellano, I. Colantoni, A. Coppolecchia, C. Cosmelli, A. D’Addabbo, S. Di Domizio, M. Martinez, C. Tomei, and M. Vignati, “Phonon-Mediated KIDs as Light Detectors for Rare-Event Search: The CALDER Project,” *Journal of Low Temperature Physics* **184**, 859–865 (2016).